# Energy landscape of the reactions governing the $Na^+$ deeply occluded state of the $Na^+/K^+$-ATPase in the giant axon of the Humboldt squid

Juan P. Castillo[a,b], Daniela De Giorgis[a,b], Daniel Basilio[a,c], David C. Gadsby[a,d], Joshua J. C. Rosenthal[a,e], Ramon Latorre[a,b,1], Miguel Holmgren[a,f,1], and Francisco Bezanilla[a,g,1]

[a]Laboratorio de Fisiologia Celular, Facultad de Ciencias, Universidad de Chile, Montemar 2366103, Chile; [b]Centro Interdisciplinario de Neurociencia de Valparaiso, Universidad de Valparaiso, Valparaiso 2366103, Chile; [c]Department of Anesthesiology, Weill Cornell Medical College, New York, NY 10065; [d]Laboratory of Cardiac/Membrane Physiology, The Rockefeller University, New York, NY 10065; [e]Department of Biochemistry, University of Puerto Rico–Medical Sciences Campus, San Juan, Puerto Rico 00901; [f]Molecular Neurophysiology Section, Porter Neuroscience Research Center, National Institute of Neurological Disorders and Stroke, National Institutes of Health, Bethesda, MD 20892; and [g]Department of Biochemistry and Molecular Biology, University of Chicago, Gordon Center for Integrative Sciences, Chicago, IL 60637

Contributed by Ramón Latorre, October 5, 2011 (sent for review August 9, 2011)

**The $Na^+/K^+$ pump is a nearly ubiquitous membrane protein in animal cells that uses the free energy of ATP hydrolysis to alternatively export $3Na^+$ from the cell and import $2K^+$ per cycle. This exchange of ions produces a steady-state outwardly directed current, which is proportional in magnitude to the turnover rate. Under certain ionic conditions, a sudden voltage jump generates temporally distinct transient currents mediated by the $Na^+/K^+$ pump that represent the kinetics of extracellular $Na^+$ binding/release and $Na^+$ occlusion/deocclusion transitions. For many years, these events have escaped a proper thermodynamic treatment due to the relatively small electrical signal. Here, taking the advantages offered by the large diameter of the axons from the squid *Dosidicus gigas*, we have been able to separate the kinetic components of the transient currents in an extended temperature range and thus characterize the energetic landscape of the pump cycle and those transitions associated with the extracellular release of the first $Na^+$ from the deeply occluded state. Occlusion/deocclusion transition involves large changes in enthalpy and entropy as the ion is exposed to the external milieu for release. Binding/unbinding is substantially less costly, yet larger than predicted for the energetic cost of an ion diffusing through a permeation pathway, which suggests that ion binding/unbinding must involve amino acid side-chain rearrangements at the site.**

P-type ATPases | pump currents | thermodynamics

During each normal transport cycle of the $Na^+/K^+$-ATPase pump, three $Na^+$ are exported from the cell in exchange for two $K^+$ imported, a process driven by hydrolysis of one molecule of ATP. By establishing the $Na^+$ and $K^+$ gradients across cell membranes, the $Na^+/K^+$ pump enables action potentials, synaptic signaling, and most solute transport in and out of cells. Two consequences of the unequal transport stoichiometry of $Na^+$ and $K^+$ are that steady pumping produces an outwardly directed current (1), proportional in magnitude to the turnover rate (2), which can be monitored electrically (3–8), and that at least one step in the transport cycle must move charge through the membrane field (9). The latter implies that, under favorable conditions, charge relaxations following voltage jumps can be used to learn details about specific steps during the transport cycle (10–28).

In the absence of internal and external $K^+$, the nominal absence of internal ADP and presence of an ATP regenerating system, the $Na^+/K^+$ pump allows exchange of $3Na^+$ between their binding sites in a deeply occluded conformation and the external milieu (21, 29) (Fig. 1*A*; encircled by dotted lines). Under these conditions there is no steady pump current observed at any voltage. Nevertheless, sudden voltage steps produce pre-steady-state currents that can be recorded (12, 13, 16–18, 21, 23, 26). These currents allow direct measurements of the rates of partial reactions of the pump cycle. Using giant axons from the squid *Loligo pealeii*, we have characterized the kinetics of extracellular $Na^+$ binding/release and $Na^+$ occlusion/deocclusion and proposed mechanistic and structural hypotheses related to ion movement (18). The time course of the transient pump currents contains a fast, a medium-speed, and a slow component (see *Materials and Methods* and ref. 18). The temporal correlation between these components indicates that they occur in strict sequence (18), likely representing the binding/release and occlusion/deocclusion of individual $Na^+$ (Fig. 1*B*). The charge distribution of each component can be described by a Boltzmann function with an apparent valence for the charge moved of approximately 1 for the medium (18) and slow (12, 13, 16–18, 21, 23, 26, 30) components but only approximately 0.2 for the fast component, indicating that it does not transport charge across a large portion of the electric field (26). Most importantly, the voltage dependence of the slow relaxation shifts with changes in external $Na^+$ concentration, $[Na^+]_o$, supporting the interpretation that $Na^+$ ions must negotiate a high-field access channel as they travel back and forth between the external solution and their binding sites deep within the $Na^+/K^+$ pump (17, 18, 23).

Giant axons from *Loligo* have provided unique advantages for studying $Na^+$ translocation events mediated by the pump (18, 29). However, they too have limits. At low temperatures the amplitudes of the signals resulting from the binding/release of extracellular $Na^+$ are too small to permit study of the thermodynamics of these steps. To overcome these biological limitations, we have performed experiments using the giant axons of the Humboldt squid (*Dosidicus gigas*). In Chile, where these experiments were conducted, these squid commonly reach lengths close to 2 m and weigh up to 40 kg. More importantly for the present purpose, their axons routinely surpass 1.2 mm in diameter (approximately twice the diameter of a large *Loligo* axon), providing a substantially larger membrane area, and hence a greater number of pumps, than comparable lengths of axons from *Loligo*. With the aim of characterizing the energetic landscape of the transitions associated with the extracellular release of the first $Na^+$ from the deeply occluded state, in this study we have determined the ther-

Author contributions: M.H. and F.B. designed research; J.P.C., D.D.G., D.B., D.C.G., J.J.C.R., M.H., and F.B. performed research; J.P.C., R.L., M.H., and F.B. analyzed data; and R.L., M.H., and F.B. wrote the paper.

The authors declare no conflict of interest.

[1]To whom correspondence may be addressed. E-mail: ramon.latorre@uv.cl, holmgren@ninds.nih.gov, or febesanilla@uchaicago.edu.

This article contains supporting information online at www.pnas.org/lookup/suppl/doi:10.1073/pnas.1116439108/-/DCSupplemental.

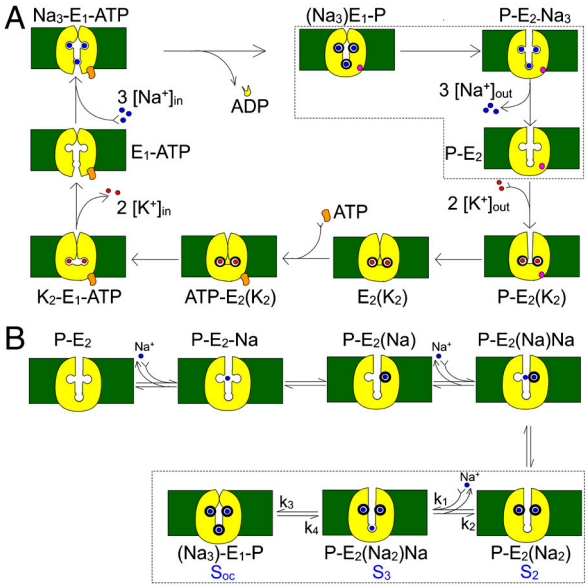


**Fig. 1.** Kinetic schemes. (*A*) Simplified Albers-Post model for the $Na^+/K^+$ pump cycle. $E_1$ and $E_2$ are the main $Na^+/K^+$ pump conformations with ion binding sites facing the intracellular and extracellular sides, respectively. Internal (0 ADP, 0 P, 0 $K^+$, and an ATP regenerating system) and external solutions (0 $Na^+$) were designed to force the pump to operate in a strictly forward direction (Fig. 3). (*B*) Explicit extracellular $Na^+$ binding/release and occlusion/deocclusion model. Electrogenic binding and release of each $Na^+$ is assumed to be independent and in strict sequence. Similarly, $Na^+$ are occluded and deoccluded independently but with electroneutral transitions. States encircled by dotted lines represent the binding/release and occlusion/deocclusion governing the slow component of the transient currents. Here we have assumed that the deep occlusion and the $E_1$-P ↔ $E_2$-P transitions are the same reaction.

modynamic parameters of the slowest component of $Na^+$ translocation.

## Results and Discussion

**$Na^+/K^+$ Pump Turnover Rate Revisited.** The effectiveness with which the $Na^+/K^+$ pump exports $Na^+$ is encapsulated by its turnover rate, which is a measure of how quickly the entire sequence of state transitions depicted in Fig. 1*A* is completed. To gauge the temperature sensitivity of the whole transport cycle, we characterized the $Na^+/K^+$ pump's turnover rate ($v_f$) as a function of temperature. Pumps were constrained to cycle in the forward direction predominantly by withholding external $Na^+$, as well as intracellular ADP, phosphate, and $K^+$ (see Fig. 1*A*). The steady-state $Na^+/K^+$ pump current was then determined, at three different voltages (−70, 0, and +40 mV), as the component of membrane current abolished by a near-saturating concentration (100 μM) of dihydrodigitoxigenin ($H_2$DTG), a specific and reversible inhibitor of squid $Na^+/K^+$ pumps (2). Corresponding values of $v_f$ at these voltages (Fig. 2) were obtained by dividing the pump current by an estimate of the total number of $Na^+/K^+$ pumps in the same axon, determined from pump charge movements (see Figs. 3 and 6 below; also see *Materials and Methods*). Under these conditions, in the absence of external $Na^+$, $v_f$ becomes essentially voltage independent (5), and for this reason we thought it reasonable to plot results obtained at different voltages together. In confirmation, $v_f$ was similar across this potential range, with values of 20–23, 67–74, or approximately 106 $s^{-1}$ at temperatures of 15.2, 22.1, and 25.3 °C, respectively. Assuming that within these voltage and temperature ranges $v_f$ reflects the same rate-limiting step, then on the basis of transition state theory the temperature dependence of $v_f$ is given by

$$\ln \nu_f = -\frac{\Delta H^{\neq}}{RT} + \frac{\Delta S^{\neq}}{R} + \ln A, \qquad [1]$$

where $\Delta H^{\ddagger}$ is the transition enthalpy, $R$ is the molar gas constant, $T$ is the absolute temperature, $\Delta S^{\ddagger}$ is the transition entropy, and $A$ is the preexponential factor of the rate. A linear regression fit to a plot of $\ln v_f$ against $1/T$ yields the slope $-\Delta H^{\ddagger}/R$ and intercept $\Delta S^{\ddagger}/R + \ln A$. From the data in Fig. 2, we estimated $\Delta H^{\ddagger}$ to be approximately 24 kcal/mol, which corresponds to a $Q_{10}$ of approximately 4.3, similar to previous reports (31–33).

The value of the transition entropy, $\Delta S^{\ddagger} = 89.8 - R \ln A$, necessarily requires a knowledge of the factor $A$, which for large molecules in aqueous solutions is largely unknown. For some protein conformational changes involved in protein folding or ion channel opening, however, experimental estimates have put the value of $A$ at approximately $10^6$ $s^{-1}$ (34, 35). With this assumption, $\Delta S^{\ddagger}$ is approximately 62 cal/molK.

Given these estimates for $\Delta H^{\ddagger}$ and $\Delta S^{\ddagger}$, we can calculate the height of the free energy barrier ($\Delta G^{\ddagger}$) that determines the rate-limiting step of forward pumping under our experimental conditions: At 15 °C it is approximately 6.1 kcal/mol, and at 25 °C it is approximately 5.5 kcal/mol. This result means that, for a 10 °C increase in temperature, pump cycling encounters only a small reduction ($<1RT$) in the barrier height. However, this small change in $\Delta G^{\ddagger}$ should not be taken to imply that the underlying structural changes are small. On the contrary, the values for $\Delta H^{\ddagger}$ and $T\Delta S^{\ddagger}$ are both large, indicating large conformational changes, although the enthalpic and entropic terms largely cancel each other.

**$Na^+$ Translocation in Giant Axons from the Humboldt Squid.** Because temperature dependence provides information on the extent of structural changes, studying the thermodynamics of isolated transitions is particularly informative. We have been able to precisely restrict a subset of transitions from the $Na^+/K^+$ pump's transport cycle that relate to the binding/release and occlusion/deocclusion of external $Na^+$. We have been studying these signals in fine detail by using electrophysiological methods (18). The signal to noise ratio in *Loligo* axons had made it difficult to estimate the thermodynamic parameters at low temperatures, because, as the total charge is conserved, the amplitude of the transient currents become small as the temperature is decreased. We have solved this problem by using axons of the squid *D. gigas* that are much larger, giving transient pump currents about 3–5 times greater than those obtained by using the largest *Loligo* axons (see below).

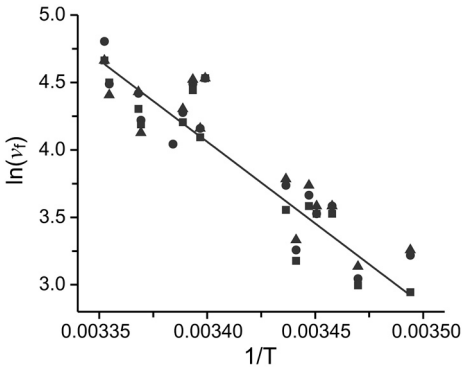


**Fig. 2.** Activation energy of the $Na^+/K^+$ forward pumping rate. Forward pump rates were estimated from 16 axons (16 $H_2$DTG-sensitive steady-state determinations) at voltages of −70 (■), 0 (●), and +40 mV (▲), with temperatures ranging from 13.2 to 25.3 °C. The solid line represents a linear fit in which the best fit parameter value for the slope and intercept were −12,103 and 45.2, respectively.

A typical experiment that isolates transient pump currents is shown in Fig. 3*A*. This experiment was performed with 400 mM $[Na^+]_o$ (roughly the concentration of sea water) and at a temperature of 27.6 °C. Records 1–3, spaced at intervals of approximately 25 s, show averages of three traces, each in response to a 25 ms voltage step to −80 mV from a holding potential of 0 mV. Pump-mediated $Na^+$ translocation (Fig. 3*B*, *Upper*) is isolated by subtracting the nonspecific membrane currents (record 2) from the total membrane current before the application of 100 μM $H_2DTG$ (record 1). Subtraction of similar current records after complete $H_2DTG$ inhibition (records 2–3) provides a time control to evaluate the stability of the preparation over the time interval needed to obtain records before and after arresting all the $Na^+/K^+$ pumps (Fig. 3*B*, *Lower*). Because we used $K^+$-free $Na^+$ solutions with high internal ATP and no ADP (see *Materials and Methods*), the transient currents shown in Fig. 3*B* reflect the kinetics of external $Na^+$ interacting with phosphorylated conformations of $Na^+/K^+$ pumps (Fig. 1*B*). These transient currents have been studied in detail by using *Loligo* axons (18). They are composed of three distinct components, which have been proposed to represent the strict sequential binding/release and occlusion/deocclusion of the three $Na^+$. The general features of the pump transient currents in *Dosidicus* are not different from those measured in *Loligo* (Figs. 3 *B* and *C*), but the amplitudes of the transient currents are substantially larger. The onset of the voltage step to −80 mV elicits a large, fast spike (Fig. 3*B*), which reflects the binding and occlusion of the first $Na^+$ (18). The medium and slow components are represented by a two-exponential fit to the subsequent current decay (Fig. 3*C*, solid red line). The slower component ($\tau \sim 1.4$ ms) is derived from the pumps populating the deeply $Na^+$ occluded state [Fig. 1*B*; $(Na_3)E_1$-P]. This component involves a voltage-dependent binding/release reaction through an access channel and an electroneutral conformational change associated with occlusion/deocclusion (18). From the reaction scheme, it is clear that the probability of entering into the deeply occluded state depends on the probability of finding the pump in the preceding state [P-$E_2(Na_2)$Na]. Therefore, assuming the $Na^+$-binding reaction is at equilibrium

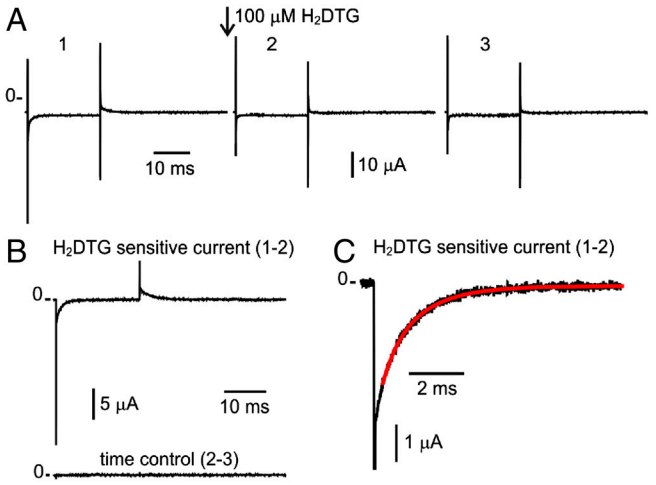


**Fig. 3.** $Na^+$ translocation by the $Na^+/K^+$-ATPase. (*A*) Current traces in response to a voltage step to −80 mV from a holding potential of 0 mV. Trace 1 was acquired immediately before the application of 100 μM $H_2DTG$ to the external solution. Trace 2 was acquired after complete pump inhibition (approximately 25 s after $H_2DTG$ application). Trace 3 was acquired approximately 25 s after trace 2. (*B*) Pump-mediated $Na^+$ translocation (*Upper*) is obtained by subtracting the nonspecific membrane current of trace 2 from trace 1. The stability of the preparation was assessed by subtracting similar time-spaced acquisitions (*Lower*). (*C*) Expanded form of the On transient current in response to the voltage step to −80 mV. The solid line represents a two-component exponential fit to the current relaxation with best fit parameter values for the time constants of 0.56 and 1.44 ms.

with respect to the occluding reaction, the rate $(1/\tau_{slow})$ is given by the relation (*SI Text*)

$$\frac{1}{\tau_{slow}} = k_s = \frac{k_3}{1 + \frac{K(0)\exp(\frac{z\delta FV}{RT})}{[Na]_o}} + k_4, \qquad [2]$$

where the $Na^+$ binding/unbinding reaction parameters are the dissociation constant at 0 mV $[K(0)]$, the $Na^+$ valence ($z$) is 1, and $\delta$ represents the electrical distance that the $Na^+$ must travel across the electric field along the access channel, whereas $k_3$ and $k_4$ denote the occlusion and deocclusion rates, respectively.

Both the forward and backward rate constants can be extracted by extending the model to extreme voltages. At very negative potentials the model predicts an asymptote given by $k_s = k_3 + k_4$ and at very positive voltages an asymptote given by $k_s = k_4$. Fig. 4 shows that as predicted a constant value for $k_s$ is reached at voltages ≥0 mV. In this experiment, performed at 31 °C, $k_s$ reaches a value of approximately 390 $s^{-1}$ at voltages ≥0 mV. The asymptote at negative potentials $(k_3 + k_4)$ can only be estimated, because these data would require voltage steps far beyond what the axon's membrane can withstand without damage ($\leq -200$ mV). The solid line shows a fit of the $k_s$ vs. $V$ data to Eq. **2** in which $\delta$ has been constrained to 0.7, a rather robust value that has been obtained by using different approaches and preparations (12, 13, 17, 18, 26, 29, 30). Fixing $\delta$ allows us estimate $k_3$ to be approximately 1,180 $s^{-1}$ at 31 °C.

**Global Fit of $k_s$ vs. Voltage at Different Temperatures.** Our aim is to determine the thermodynamic parameters that characterize the slow component, because it represents the rate-limiting transition for external $Na^+$ translocation. The temperature dependence of $k_s$ (Eq. **2**) may be obtained on the basis of transition state theory for $k_3$ and $k_4$ and by assigning enthalpic and entropic components to the binding/unbinding reactions to give (see *SI Text*)

$$k_s = A\exp\left(\frac{-\Delta H_4^{\neq} + T\Delta S_4^{\neq}}{RT}\right) + \frac{A\exp(\frac{-\Delta H_3^{\neq} + T\Delta S_3^{\neq}}{RT})}{1 + \frac{C^0}{[Na]_o}\exp(\frac{z\delta FV - \Delta H_u + T\Delta S_u}{RT})}, \qquad [3]$$

where $\Delta H^{\neq}$ and $\Delta S^{\neq}$ correspond to the activation enthalpies and entropies for the deocclusion (subindices 4) and occlusion (subindices 3), respectively, $A$ is the preexponential term, which has been set to be $10^6$ $s^{-1}$ (34, 35) and assumed to be the same for the slow deocclusion and occlusion reactions, $C^0$ is the standard state concentration of 1 mol/L (=1/1661 $Å^3$; see ref. 36), and $\Delta H_u$ and $\Delta S_u$ are the total enthalpy and entropy, respectively,

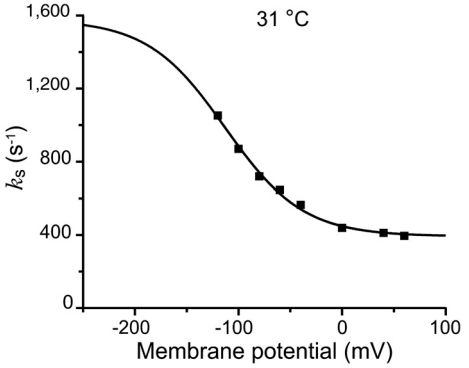


**Fig. 4.** Voltage dependence of the relaxations of the slow charge translocation component. The solid line represents a fit of the data to Eq **2**. The best fit parameter values for $k_3$, $k_4$, and $K(0)$ were 1,185 $s^{-1}$, 393 $s^{-1}$, and 8.16 M, respectively.

of the adjacent binding reaction (binding of the third $Na^+$ and unbinding of the first $Na^+$ released).

To determine the parameters of Eq. **3**, we first measured the slow time constant ($\tau_{slow}$) of 151 $H_2$DTG-sensitive pre-steady-state currents obtained from voltages between −120 and +60 mV and temperatures ranging from 16.8 to 32.2 °C. Second, the reciprocals of the experimental time constants ($k_s = 1/\tau_{slow}$) were globally fitted to Eq. **3** to extract the entropies and enthalpies of the third $Na^+$ binding/unbinding and the occlusion/deocclusion reactions. All the experiments were performed with 400 mM $[Na]_o$. As before, $\delta$ was the only fixed parameter. Because the fit was made by using every relaxation rate at a given temperature and membrane potential, it is difficult to present all the data, together with the fits, in a single panel. For presentation purposes, Fig. 5 shows the data binned in four temperature ranges, each spanning less than about 2 °C (as indicated in Fig. 5). The average experimental rates at each potential, in each temperature bin, are shown with their standard deviation. The curves in Fig. 5 were generated by assigning the fitted parameters to Eq. **3** and using temperature values representing the average of each bin.

The results from the fit are summarized in Table 1 (bold) along with the derived parameters. These results provide insights into the energy landscapes of the transitions involving the deeply occluded conformation. The occlusion/deocclusion transition of the first $Na^+$ to be released from the pump involves large enthalpic and entropic changes (Net $\Delta H = 19.6$ kcal/mol and net $\Delta S = 62.4$ cal/mol K). From the occlusion/deocclusion net enthalpy, it is expected that this transition would have a $Q_{10}$ value of 3.3 (18, 22), characteristic of transitions involving protein conformational changes. Of note is the fact that it is smaller than the value obtained for the rate-limiting step ($v_f$) when $Na^+/K^+$ pumps are exchanging $Na^+$ for $K^+$ (Fig. 2) in their normal mode of operation, indicating that release of the deeply occluded $Na^+$ is not the step that rate limits the pump cycle. Likely, completion of the entire transport cycle is limited by transitions associated with dephosphorylation and deocclusion of $K^+$ to the intracellular side, which involve large conformational changes of intracellular domains that are accelerated by low-affinity binding of ATP (37). In addition, the thermodynamic analysis of the $Na^+$ occlusion/deocclusion step indicates that the energetic landscape of this transition is not symmetrical. Thus, assuming that the transition state is the same for the deep occlusion and deocclusion reactions, considerably more activation energy seems required to leave the deeply occluded state ($\Delta H_4^{\neq} = 23.6$ kcal/mol; $Q_{10} = 4.2$) than to return ($\Delta H_3^{\neq} = 4.3$ kcal/mol; $Q_{10} = 1.3$). In spite of this fact, the heights of the free energy barriers are not very different in the two directions. If anything, the deeply occluded state [P-$E_1(Na_3)$] is slightly more stable than the P-$E_2(Na_2)\cdot Na$ state. The increase in net entropy of the occlusion/deocclusion transition indicates that the deeply occluded state is also more ordered than the P-$E_2(Na_2)\cdot Na$ state.

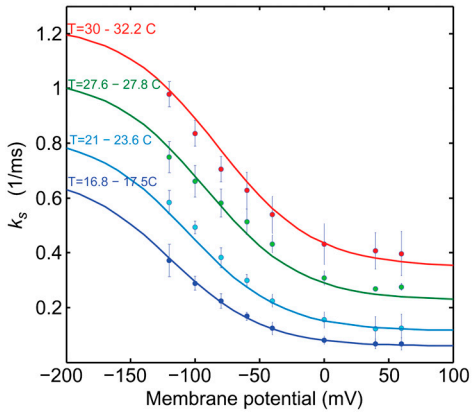


**Fig. 5.** Global fit of the slow rate constant $k_s$, as a function of voltage. A total of 151 reciprocal slow time constants that spanned 8 voltages and 15 temperatures were fitted to Eq **3**. The data have been grouped at four temperatures, and the points represent averages with their standard deviation. The continuous curves were generated with the fitted parameters at the average value of each group of temperatures. The range of temperatures of each group is indicated at the left of the graph.

The adjacent $Na^+$ binding/release transition has a smaller enthalpy (net $\Delta H = -11.4$ kcal/mol), which corresponds to a $Q_{10}$ of only 2.0. Such levels of enthalpic activation energy are consistent with processes that do not require conformational changes as substantial as those associated with occlusion/deocclusion reactions, as might be expected for a $Na^+$ traveling through an access channel and interacting with its binding site. For comparison, in open voltage-gated $Na^+$ channels, $Na^+$ permeation causes even smaller changes in enthalpy (6.25 kcal/mol; $Q_{10} = 1.53$) (38) or $K^+$ binding to the $Na^+/K^+$-ATPase where values of $Q_{10}$ are approximately 1.3 (22, 39). This smaller value, in turn, suggests that the binding and unbinding reaction of this $Na^+$ to the $Na^+/K^+$-ATPase itself involves amino acid rearrangements. Interestingly, the decrease in entropy upon unbinding implies that the unbound state [P-$E_2(Na_2)$] is more ordered than the bound state [P-$E_2(Na_2)\cdot Na$]; possibly, release of that $Na^+$ might allow ordered binding of water molecules, thus lowering the electric field for subsequent release of the two remaining $Na^+$ (9, 18, 26, 28).

The overall net change in free energy over the two coupled transitions ($S_{oc} \leftrightarrow S_2$) is essentially zero, indicating that under the conditions of these experiments the occluded $(Na_3)E_1$-P and partly deoccluded P-$E_2(Na_2)$ states are energetically equivalent. The net $\Delta H$ and $\Delta S$ values of these combined transitions (Table 1) are poorly determined, because the confidence in the $\Delta H$ and $\Delta S$ values is low. However, we extract from the net $\Delta H$ a $Q_{10}$ of 1.6 for the overall reaction on the basis of the enthalpic change. Of more interest is that the effect of temperature on the voltage dependence of the charge moved between $(Na_3)E_1$-P and P-$E_2(Na_2)$ states can be predicted and checked against the $Q$-$V$ curves. The shift of the midpoint of the distribution of the charge vs. potential with temperature is a direct indication of an entropic change in the overall reaction (38). When we consider only the net changes in entropy and enthalpy, we derive the midpoint of the distribution ($V_{1/2}$) of the charge vs. potential curve from a two-state model (see *SI Text*) as

$$V_{1/2} = \frac{\Delta H_T - T\Delta S_T + RT\ln([Na]/C^0)}{z\delta F}. \qquad [4]$$

From the net $\Delta S$ obtained from the global fit (see Table 1), increasing the temperature by 10 °C is expected to shift the charge distribution by approximately 17 mV toward negative voltages. Indeed, we did observe a small negative shift of $V_{1/2}$ upon increasing the temperature (Fig. 6). The measured shift, however, is somewhat smaller than predicted. It should be noted that the midpoints of $Q$-$V$ relationships under our experimental conditions are difficult to determine with precision, because charge movement at voltages near the holding potential cannot be accurately measured. With this difficulty in mind, it is significant that the direction of the predicted shift is fulfilled by the direct measurements of the charge distribution vs. potential. Although the direction of the $Q$-$V$ curve displacement with temperature might appear counterproductive for a squid neuron subjected to a decrease in temperature, because $Na^+$ release would then be hindered, our results indicate that the effect is too small to have any real consequences for intracellular ion homeostasis.

**Conclusions.** Electrophysiological studies of external $Na^+$ translocation by the $Na^+/K^+$-ATPase have deepened our understanding of how external $Na^+$ are bound and released (10, 11, 13–19, 21, 23–27, 29, 30), and they have provided a picture of the general

**Table 1. Thermodynamic parameters describing the reactions governing the $Na^+$ deeply occluded state**

| | | $\Delta H^{\neq}$ kcal/mol | $\Delta S^{\neq}$ cal/molK | $\Delta G^{\neq}$ kcal/mol | Net $\Delta H$ kcal/mol | *Net* $\Delta S$ *cal/mol K* | Net $\Delta G$ kcal/mol |
|---|---|---|---|---|---|---|---|
| $S_{oc} \leftrightarrow S_3$ | deocclusion | **23.6 ± 1.5** | **61.8 ± 5.1** | 5.5 ± 1.7 | 19.6 | *62.4* | 1.2 ± 1.5 |
| | occlusion | **(4.1 ± 1.3)** | **(−0.6 ± 4.5)** | **4.3 ± 0.1** | | | |
| Binding/unbinding $S_3 \leftrightarrow S_2$ $K(0) = 7.74 \pm 0.6$ | | | | | **−11.4 ± 3.5** | **−34.7 ± 12** | −1.2 ± 3.5 |
| Combined $S_{oc} \leftrightarrow S_2$ | | | | | 8.4 | *27.7* | 0 ± 3.8 |

architecture of the path through which $Na^+$ move between their binding sites and the external milieu: the access channel model (9, 17, 18, 23, 26, 29). The energetic landscape of the transitions associated with the extracellular release of the first $Na^+$ from the deeply occluded state revealed that the occlusion/deocclusion transition involves large changes in enthalpy and entropy as the ion is exposed to the external milieu for release. Clearly, ion unbinding must carry some amino acid side-chain rearrangements at the site, because the enthalpic activation energy of the binding/unbinding reaction was substantially larger than expected for an ion diffusing through a permeation pathway. This study provides the initial framework for further investigations on the energetic landscape for the release of the second and third $Na^+$, to begin building a precise description of the molecular events that accompany the translocation of $Na^+$ by the $Na^+/K^+$-ATPase.

## Materials and Methods

**Squid Collection and Axon Preparation.** Humboldt squid (*D. gigas*) were caught by local fishermen using traditional methods. Once a large specimen was brought on the boat, a large section of the mantle containing the stellate ganglion and giant axons of both sides was immediately excised and transferred to an insulated container filled with chilled sea water. Within 30 min, axons were removed from the mantle, separated, and kept in filtered sea water in a refrigerator at 4 °C. Healthy axons could be kept up to 2 d. As needed, axons were cleaned prior to experiments.

**Experimental Solutions.** Giant axons were internally dialyzed and externally superfused with solutions designed to allow the $Na^+/K^+$-ATPases either to cycle at maximum speed in the forward direction (Fig. 1*A*) or to distribute themselves among conformations connected by reversible transitions involving the binding/unbinding and occlusion/deocclusion of external $Na^+$ (Fig. 1*B*). In both cases, the dialysis solution was prepared from stock solutions (pH 7.6, adjusted with Hepes) and contained (in millimoles): 85 Na-Hepes, 80 *N*-methyl-D-glucamine (NMDG)-Hepes, 50 glycine, 50 phenylpropyltriethyl-ammonium sulfate [to block potassium channels (40)], five DTT, 2.5 1,2-bis(2-aminophenoxy)ethane-*N,N,N′,N′*-tetraacetate, 10 Mg-Hepes, 5 Mg-ATP, five phospho(enol) pyruvate tri-$Na^+$ salt, and five phospho-L-arginine mono-$Na^+$ salt. Turnover rate experiments were performed with external solutions containing (in millimoles): 400 tetra methylammonium (TMA)-sulfamate, 10 KCl, 75 $Ca^{2+}$-sulfamate, 1 3,4-diaminopyridine, $2 \times 10^{-4}$ TTX, 5 Tris-Hepes, and 0.05 EDTA (pH 7.7, adjusted with NMDG or sulfamic acid). In experiments to study external $Na^+$ charge translocation, the external solutions had 400 Na-sulfamate instead of TMA-sulfamate and were devoid of KCl. During the last experimental season in Chile, external solutions contained chloride instead of sulfamate as the anion. These changes did not cause detectable differences either in the electrical leak of the preparation or in the kinetics of the $Na^+$ translocation. The osmolality of all solutions was adjusted to approximately 950 mOsmol $kg^{-1}$.

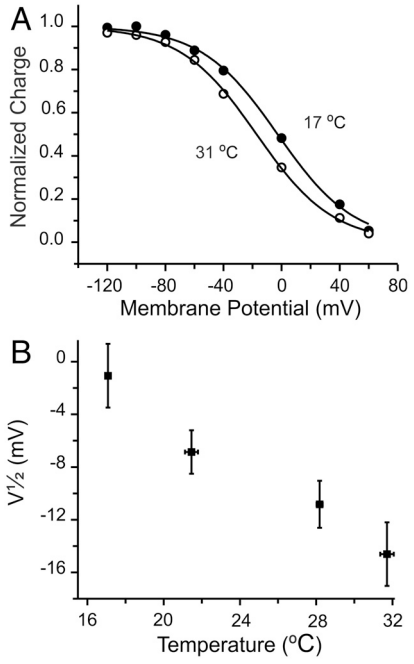


**Fig. 6.** Influence of temperature on the voltage dependence of charge distribution. (*A*) Charge distributions. Normalized charge moved by the slow component from an axon exposed at 17 (●) and 31 °C (○). Solid lines represent Boltzmann fits with midpoint values of −3 ± 1 (17 °C) and −17 ± 1 mV (31 °C). (*B*) Shift of voltage dependence with temperature. Data were grouped similarly as in Fig. 5.

**Axon Preparation and Electrophysiology.** Freshly dissected giant axons (950- to 1,200-μm diameter) were threaded through a chamber that contained a central test pool flanked by two guard pools. The three pools have independent inlet and outlet perfusion systems. A peltier block controls the temperature of the solution before it enters the chamber, and the block is also in thermal contact with the three chamber pools. A thermocouple within the block feeds back to a temperature regulation system on the basis of an Omega controller. A microthermocouple measures the temperature in the test pool near the axon. Once the axon is mounted, it is cut at both ends, and the dialysis system comprising two 210-μm porous capillaries, each containing a 100-μm platinized platinum wire, is inserted and advanced along the entire axon length. The internal voltage electrode (a 120-μm glass capillary filled with 0.6 M KCl solution and containing an electrically floating platinum wire) is inserted as far as the middle of the axon (i.e., within the central pool). The external reference electrode, a 3M KCl/agar-filled glass capillary that also contains a floating platinum wire, is placed in the central pool just outside the axon and near the solution outflow. The current is collected in the central chamber by a large platinized platinum plate connected to a current-to-voltage converter that keeps the compartment at virtual ground, whereas the guard chambers are connected directly to ground through two additional large platinized platinum plates (41). Voltage steps were generated, and currents recorded, by using a 14-bit high speed analog-digital–digital-analog conversion board (A4D1; Innovative Integration) driven by a SB6711 board (Innovative Integration) with software developed in house. Currents were filtered at 100 kHz with an eight-pole Bessel filter (Frequency Devices 90IP or Krohn-Hite 3382) and then sampled at 3 μs intervals. The pump-mediated currents were isolated by using $H_2$DTG to specifically and reversibly inhibit squid $Na^+/K^+$ pumps (2). $H_2$DTG-sensitive currents were analyzed with in-house software and OriginLab v8. Global fits were carried out with programs written in Matlab utilizing their fit library.

**Turnover Rate Estimations.** Steady-state $Na^+/K^+$ pump currents, and the number of $Na^+/K^+$ pumps generating them, were determined independently in each axon. $Na^+/K^+$-ATPase density was estimated from the total amount of charge moved during $Na^+$ translocation transitions between −120 and +60 mV, at room temperature, assuming that the equivalent of a single charge moves through the entire membrane electric field. Under the conditions of these recordings, >90% of the total amount of charge is moved (18). Steady-state pump currents were measured at voltages of −70, 0, and +40 mV, in the presence of 10 mM external $K^+$ and the nominal absence of external $Na^+$. Each steady-state pump current measurement was bracketed with two estimates of pump density assessed by the maximum amount of $Na^+$ translocation charge. The pump density at the time of the steady-state current measurement was interpolated when necessary. The turnover rate is simply the steady-state pump current divided by the total amount of $Na^+$ translocation charge.

**ACKNOWLEDGMENTS.** We kindly thank Francisco Palma, who during the first two experimental seasons participated in the squid collection and performed, in the boat, the first step of the animal dissection. We also thank Professor Mario Luxoro, Alan Neely, Ana Maria Navia, Rodrigo Toro, and Jose Soto for in situ logistics throughout the years that facilitate and maximize our short experimental season in Montemar. We thank the Section on Instrumentation of the National Institute of Mental Health for technical assistance. This work was possible thanks to Fogarty International Research Collaboration Award Grant RO3 TW008351 (to R.L., F.B., and M.H.). F.B. was supported by National Institutes of Health (NIH) (U54GM087519 and R01GM030376). J.J.C.R. was supported by NIH (R01NS64259). R.L. was supported by Fondo Nacional de Desarrollo Científico y Tecnológico Grant 1110430. The Centro Interdisciplinario de Neurociencia de Valparaiso is a Scientific Millennium Institute. D.C.G. was supported by NIH (R01HL36783). This study was also partially supported by the Intramural Research Program of the NIH (National Institute of Neurological Disorders and Stroke). D.B. thanks the Albert Cast Traveling Fellowship for providing travel funds to Montemar, Chile (2009 season).

1. Gadsby DC, Kimura J, Noma A (1985) Voltage dependence of Na/K pump current in isolated heart cells. *Nature* 315:63–65.
2. Rakowski RF, Gadsby DC, De Weer P (1989) Stoichiometry and voltage dependence of the sodium pump in voltage-clamped, internally dialyzed squid giant axon. *J Gen Physiol* 93:903–941.
3. Gadsby DC, Nakao M (1989) Steady-state current-voltage relationship of the Na/K pump in guinea pig ventricular myocytes. *J Gen Physiol* 94:511–537.
4. Goldshlegger R, Karlish SJ, Rephaeli A, Stein WD (1987) The effect of membrane potential on the mammalian sodium-potassium pump reconstituted into phospholipid vesicles. *J Physiol* 387:331–355.
5. Nakao M, Gadsby DC (1989) [Na] and [K] dependence of the Na/K pump current-voltage relationship in guinea pig ventricular myocytes. *J Gen Physiol* 94:539–565.
6. Rakowski RF, Paxson CL (1988) Voltage dependence of Na/K pump current in Xenopus oocytes. *J Membr Biol* 106:173–182.
7. Rakowski RF, Vasilets LA, LaTona J, Schwarz W (1991) A negative slope in the current-voltage relationship of the $Na^+/K^+$ pump in Xenopus oocytes produced by reduction of external [$K^+$]. *J Membr Biol* 121:177–187.
8. Sagar A, Rakowski RF (1994) Access channel model for the voltage dependence of the forward-running $Na^+/K^+$ pump. *J Gen Physiol* 103:869–893.
9. Läuger P (1991) *Electrogenic Ion Pumps* (Sinauer, Sunderland, MA).
10. Apell HJ, Borlinghaus R, Läuger P (1987) Fast charge translocations associated with partial reactions of the Na,K-pump: II. Microscopic analysis of transient currents. *J Membr Biol* 97:179–191.
11. Borlinghaus R, Apell HJ, Läuger P (1987) Fast charge translocations associated with partial reactions of the Na,K-pump: I. Current and voltage transients after photochemical release of ATP. *J Membr Biol* 97:161–178.
12. Colina C, Palavicini JP, Srikumar D, Holmgren M, Rosenthal JJ (2010) Regulation of $Na^+/K^+$ ATPase transport velocity by RNA editing. *PLoS Biol* 8:e1000540.
13. Colina C, et al. (2007) Structural basis of $Na^+/K^+$-ATPase adaptation to marine environments. *Nat Struct Mol Biol* 14:427–431.
14. Fendler K, Grell E, Bamberg E (1987) Kinetics of pump currents generated by the $Na^+$, $K^+$-ATPase. *FEBS Lett* 224:83–88.
15. Fendler K, Grell E, Haubs M, Bamberg E (1985) Pump currents generated by the purified $Na^+K^+$-ATPase from kidney on black lipid membranes. *EMBO J* 4:3079–3085.
16. Holmgren M, Rakowski RF (1994) Pre-steady-state transient currents mediated by the Na/K pump in internally perfused Xenopus oocytes. *Biophys J* 66:912–922.
17. Holmgren M, Rakowski RF (2006) Charge translocation by the $Na^+/K^+$ pump under $Na^+/Na^+$ exchange conditions: Intracellular $Na^+$ dependence. *Biophys J* 90:1607–1616.
18. Holmgren M, et al. (2000) Three distinct and sequential steps in the release of sodium ions by the $Na^+/K^+$-ATPase. *Nature* 403:898–901.
19. Kane DJ, et al. (1997) Stopped-flow kinetic investigations of conformational changes of pig kidney $Na^+$, $K^+$-ATPase. *Biochemistry* 36:13406–13420.
20. Nagel G, Fendler K, Grell E, Bamberg E (1987) $Na^+$ currents generated by the purified $Na^+/K^+$-ATPase on planar lipid membranes. *Biochim Biophys Acta* 901:239–249.
21. Nakao M, Gadsby DC (1986) Voltage dependence of Na translocation by the Na/K pump. *Nature* 323:628–630.
22. Peluffo RD, Berlin JR (1997) Electrogenic $K^+$ transport by the $Na^+$-$K^+$ pump in rat cardiac ventricular myocytes. *J Physiol* 501:33–40.
23. Rakowski RF (1993) Charge movement by the Na/K pump in Xenopus oocytes. *J Gen Physiol* 101:117–144.
24. Bühler R, Stürmer W, Apell HJ, Läuger P (1991) Charge translocation by the Na, K-pump: I. Kinetics of local field changes studied by time-resolved fluorescence measurements. *J Membr Biol* 121:141–161.
25. Heyse S, Wuddel I, Apell HJ, Stürmer W (1994) Partial reactions of the Na,K-ATPase: Determination of rate constants. *J Gen Physiol* 104:197–240.
26. Hilgemann DW (1994) Channel-like function of the Na,K pump probed at microsecond resolution in giant membrane patches. *Science* 263:1429–1432.
27. Stürmer W, Bühler R, Apell HJ, Läuger P (1991) Charge translocation by the Na,K-pump: II. Ion binding and release at the extracellular face. *J Membr Biol* 121:163–176.
28. Wuddel I, Apell HJ (1995) Electrogenicity of the sodium transport pathway in the Na, K-ATPase probed by charge-pulse experiments. *Biophys J* 69:909–921.
29. Gadsby DC, Rakowski RF, De Weer P (1993) Extracellular access to the Na,K pump: Pathway similar to ion channel. *Science* 260:100–103.
30. Peluffo RD (2004) Effect of ADP on $Na^+$-$Na^+$ exchange reaction kinetics of Na,K-ATPase. *Biophys J* 87:883–898.
31. Apell HJ (1997) Kinetic and energetic aspects of $Na^+/K^+$-transport cycle steps. *Ann NY Acad Sci* 834:221–230.
32. Friedrich T, Bamberg E, Nagel G (1996) $Na^+$, $K^+$-ATPase pump currents in giant excised patches activated by an ATP concentration jump. *Biophys J* 71:2486–2500.
33. Galarza-Munoz G, Soto-Morales SI, Holmgren M, Rosenthal JJ (2011) Physiological adaptation of an Antarctic $Na^+/K^+$-ATPase to the cold. *J Exp Biol* 214:2164–2174.
34. Yang WY, Gruebele M (2003) Folding at the speed limit. *Nature* 423:193–197.
35. Chakrapani S, Auerbach A (2005) A speed limit for conformational change of an allosteric membrane protein. *Proc Natl Acad Sci USA* 102:87–92.
36. Woo HJ, Roux B (2005) Calculation of absolute protein-ligand binding free energy from computer simulations. *Proc Natl Acad Sci USA* 102:6825–6830.
37. Post RL, Hegyvary C, Kume S (1972) Activation by adenosine triphosphate in the phosphorylation kinetics of sodium and potassium ion transport adenosine triphosphatase. *J Biol Chem* 247:6530–6540.
38. Correa AM, Bezanilla F, Latorre R (1992) Gating kinetics of batrachotoxin-modified $Na^+$ channels in the squid giant axon. Voltage and temperature effects. *Biophys J* 61:1332–1352.
39. Bühler R, Apell HJ (1995) Sequential potassium binding at the extracellular side of the Na,K-pump. *J Membr Biol* 145:165–173.
40. Armstrong CM (1971) Interaction of tetraethylammonium ion derivatives with the potassium channels of giant axons. *J Gen Physiol* 58:413–437.
41. Bezanilla F, Taylor RE, Fernandez JM (1982) Distribution and kinetics of membrane dielectric polarization. 1. Long-term inactivation of gating currents. *J Gen Physiol* 79:21–40.